12th AIAA Aviation Technology, Integration, and Operations (ATIO) Conference and 14th AIAA/ISSM
17 - 19 September 2012, Indianapolis, Indiana

AIAA 2012-5598

A Coupled-Adjoint Method for Aerodynamic and Aeroacoustic Optimization

Thomas D. Economon*, Francisco Palacios†, and Juan J. Alonso‡
Stanford University, Stanford, CA 94305, U.S.A.

Designing quieter, more efficient aerospace systems will require coupled, high-fidelity analysis and optimization in the areas of aerodynamics and aeroacoustics. This paper presents a design methodology for addressing these two disciplines within a single framework. After detailing the governing flow and time-accurate continuous adjoint equations for unsteady aerodynamics, a continuous adjoint formulation for the control of noise is developed. In order to obtain the required remote sensitivity information for an off-body observer of noise, the adjoint formulations for aerodynamics and aeroacoustics are related through a coupling boundary condition. The result is an efficient, adjoint-based methodology for design problems involving both aerodynamic performance and noise control. Furthermore, the coupled-adjoint method could be applied to other multiphysics problems where adjoint sensitivities are desired.

Nomenclature

Variable Definition

c	Speed of sound
$\vec{d}$	Force projection vector
f	Function describing the acoustic surface, $f = 0$
j_S	Scalar function defined at each point on S
$\vec{n}$	Normal vector
p	Static pressure
p_∞	Freestream pressure
p'	Acoustic pressure, $p' = p - p_\infty$
t_o	Initial time
t_f	Final time
$\vec{u}_b$	Control volume boundary velocity (mesh velocity)
$\vec{v}$	Flow velocity vector
v_∞	Freestream velocity
$\vec{A}$	Inviscid flux Jacobian matrices
A_z	Projected area in the z-direction
C_D	Coefficient of drag
C_L	Coefficient of lift
C_{SF}	Coefficient of side-force
E	Total energy per unit mass
$\vec{F}$	Euler convective fluxes
$\vec{F}_{mov}$	Euler convective fluxes in ALE form
H	Stagnation enthalpy
$\bar{\bar{I}}$	Identity matrix
$\mathcal{I}$	Objective function for the aeroacoustic problem

*Ph.D. Candidate, Department of Aeronautics & Astronautics, AIAA Student Member.
†Engineering Research Associate, Department of Aeronautics & Astronautics, AIAA Member.
‡Associate Professor, Department of Aeronautics & Astronautics, AIAA Senior Member.

$\mathcal{J}$	Objective function for the aerodynamic problem
M_∞	Freestream Mach number
$\mathcal{N}(\rho')$	Governing wave equation for acoustics
$\mathcal{Q}$	Source term(s)
$\mathcal{R}(U)$	System of governing flow equations
S	Solid wall flow domain boundary (design surface)
T	Time interval, $t_f - t_o$
U	Vector of conservative variables
W	Vector of characteristic variables
α	Angle of attack
β	Sideslip angle
γ	Ratio of specific heats, $\gamma = 1.4$ for air
ρ	Fluid density
ρ_∞	Freestream density
ρ'	Acoustic density, $\rho' = \rho - \rho_\infty$
ϕ	Acoustic adjoint variable
$\vec{\varphi}$	Flow adjoint velocity vector
Γ	Domain boundary
Ψ	Vector of flow adjoint variables
Ω	Problem domain

Mathematical Notation

$\vec{b}$	Spatial vector $b \in \mathbb{R}^n$, where n is the dimension of the physical cartesian space (in general, 2 or 3)
B	Column vector or matrix B, unless capitalized symbol clearly defined otherwise
$\vec{B}$	$\vec{B} = (B_x, B_y)$ in two dimensions or $\vec{B} = (B_x, B_y, B_z)$ in three dimensions
$\nabla(\cdot)$	Gradient operator
$\nabla \cdot (\cdot)$	Divergence operator
$\nabla^2(\cdot)$	Laplacian operator
$\partial_n(\cdot)$	Normal gradient operator at a surface point, $\vec{n}_S \cdot \nabla(\cdot)$
$\nabla_S(\cdot)$	Tangential gradient operator at a surface point, $\nabla(\cdot) - \partial_n(\cdot)$
$\cdot$	Vector inner product
$\times$	Vector cross product
$\otimes$	Vector outer product
B^T	Transpose operation on column vector or matrix B
$\delta(\cdot)$	Denotes first variation of a quantity, unless otherwise specified as the Dirac delta function

I. Introduction and Motivation

Environmental pressures to decrease fuel burn, emissions, and noise continue to drive the need for quieter, more efficient aircraft and aircraft propulsion technology. These environmental challenges also offer an opportunity for the aircraft designer to take advantage of synergistic interactions between components of the configuration design. One example of this interaction effect involves the installation of next generation propulsion systems, such as the open rotor engine, which may be more efficient at the cost of increased noise. New proposals for unconventional aircraft configurations or engine placement may target enhanced aerodynamic performance, noise shielding, or provide safety in the event of blade-out. These complex systems will require multidisciplinary, high-fidelity analysis and system-level integration studies in order to assess their viability. Other challenges might include reducing airframe or jet noise without incurring performance penalties for a particular vehicle.

The development of revolutionary technology comes hand in hand with the issue of how to optimize and integrate it. Successful deployment of new technology will require novel multidisciplinary design, analysis, and optimization (MDAO) approaches for complex aerospace systems that are rooted in physics-based predictions. As mentioned, two disciplines of particular interest are aerodynamics and aeroacoustics. High-fidelity analysis and design tools will be needed to understand the interaction between these disciplines and to aid the designer in extracting the best performance with minimal noise penalties. With a final objective of performing shape design, computational fluid dynamics (CFD) and computational aeroacoustics (CAA)

are two candidate toolsets for this type of multidisciplinary research.

In the context of optimal shape design, adjoint-based formulations have a rich history in aeronautics, and their effectiveness for the design of aircraft configurations in cruise and other steady problems is well established [1–3]. Less common and more difficult are adjoint formulations for unsteady aerodynamic problems, in part due to prohibitive data storage requirements. Recent work has demonstrated the viability of unsteady adjoint approaches for airfoil applications [4] and more complex flows on dynamic meshes [5].

Sound is an inherently unsteady phenomenon, and there exists a wealth of literature on methods for aeroacoustic analysis. While it is possible to directly compute acoustics using CFD alone, the two disciplines are often considered separately, as they will be in this article, for computational efficiency, accuracy, or flexibility reasons. Typical CAA solution procedures include coupling CFD solvers to finite element or boundary integral methods for solving the wave equation in order to compute an acoustic response. For instance, if the noise at some far-field location is desired, extending a computational mesh of fine enough resolution to preserve small acoustic waves many body-lengths away would be computationally infeasible. When approached in this manner, aeroacoustic analysis becomes a coupled, multiphysics problem requiring two separate partial differential equation (PDE) solvers for each discipline.A benefit of this approach is the flexibility to use higher fidelity (CFD) where needed to capture sound generation processes while leaving the propagation, reflection, or scattering to a less costly model (CAA). While the analysis problem has received much attention, design problems involving aeroacoustics have not, and there are limited examples of techniques that consider acoustics for shape design [6]. In a multiphysics scenario, it might be unclear how to couple the disciplines in order to exchange the sensitivity information that is needed for design.

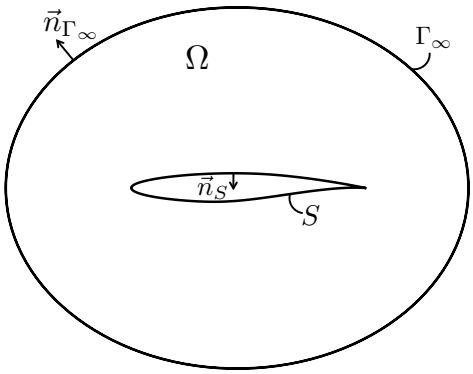

Figure 1. Notional schematic of the flow domain, Ω, and the disconnected boundaries with their corresponding surface normals, S and Γ_∞.

With this article, we present time-accurate continuous adjoint formulations for both aerodynamics and aeroacoustics and couple them together to enable shape design using remote sensitivities for controlling noise at an off-body observer location. The key to coupling the disciplines is a new adjoint boundary condition relating the local adjoint variables at the interface between the CFD and CAA domains. The coupled-adjoint technique is demonstrated through an exercise in aeroacoustic shape design.

The paper is organized as follows. Section II details the governing equations for the flow problem along with a time-accurate continuous adjoint formulation for aerodynamic shape design. In Section III, an inhomogeneous wave equation governing aerodynamically generated sound is described. This section also contains a continuous adjoint formulation for the control of noise. The method for coupling the aerodynamic and aeroacoustic adjoint problems through a boundary condition is presented in Section IV. Sections V & VI contain numerical implementation details and results, including a verification and validation of the unsteady flow and adjoint equations, as well as a demonstration of obtaining remote sensitivities for controlling the noise induced by a pitching airfoil in still air.

II. Governing Flow and Adjoint Equations for Unsteady Aerodynamics

This section contains a summary of the governing flow equations and the corresponding time-accurate continuous adjoint formulation for the aerodynamic analysis and design portion of this MDAO problem.

A. Description of the Aerodynamic Problem

Ideal fluids are governed by the Euler equations. In our particular problem, these equations are considered in a domain, Ω, bounded by a disconnected boundary which is divided into a far-field component, Γ_∞, and a solid wall boundary, S, as seen in Fig. 1. The surface S will also be referred to as the design surface, and it is considered continuously differentiable (C^1). Normal vectors to the boundary surfaces are directed out of the domain by convention.

We are interested in the time-accurate fluid behavior around aerodynamic bodies in arbitrary motion for situations where viscous effects can be considered negligible. The governing flow equations in the limit of vanishing viscosity are the compressible Euler equations. These conservation equations can be expressed in an arbitrary Lagrangian-Eulerian (ALE) differential form as

$$\begin{cases} \mathcal{R}(U) = \frac{\partial U}{\partial t} + \nabla \cdot \vec{F}_{mov} = 0, & \text{in } \Omega, \quad t_o \leq t \leq t_f \\ (\vec{v} - \vec{u}_b) \cdot \vec{n}_S = 0, & \text{on } S, \quad t_o \leq t \leq t_f \\ (W)_+ = W_\infty, & \text{on } \Gamma_\infty, \quad t_o \leq t \leq t_f \end{cases} \tag{1}$$

where

$$U = \begin{Bmatrix} \rho \\ \rho\vec{v} \\ \rho E \end{Bmatrix}, \ \vec{F}_{mov} = \begin{Bmatrix} \rho(\vec{v} - \vec{u}_b) \\ \rho\vec{v} \otimes (\vec{v} - \vec{u}_b) + \bar{\bar{I}}p \\ \rho E(\vec{v} - \vec{u}_b) + p\vec{v} \end{Bmatrix}, \tag{2}$$

ρ is the fluid density, $\vec{v} = \{u, v, w\}^T$ is the flow velocity, $\vec{u}_b$ is the boundary velocity for a control volume in motion (mesh velocity), E is the total energy per unit mass, and p is the static pressure. The second line of Eqn. 1 represents the flow tangency condition at a solid wall, and the final line represents a characteristic-based boundary condition at the far-field where the fluid state at the boundary is updated using the state at infinity depending on the sign of the eigenvalues. The boundary conditions take into account any boundary velocity due to grid motion. The temporal conditions will be problem dependent, and for purposes of this article, we will be interested in periodic flows where the initial and terminal conditions do not affect the time-averaged behavior. In order to close the system of equations after assuming a perfect gas, the pressure is determined from

$$p = (\gamma - 1)\rho \left[E - \frac{1}{2}(\vec{v} \cdot \vec{v}) \right], \tag{3}$$

and the stagnation enthalpy is given by

$$H = E + \frac{p}{\rho}. \tag{4}$$

B. Surface Sensitivities via a Time-Accurate Continuous Adjoint Approach

The objective of this section is to describe the way in which we quantify the influence of geometric modifications on the pressure distribution at a solid surface in the flow domain.

A typical shape optimization problem seeks the minimization of a certain cost function, $\mathcal{J}$, with respect to changes in the shape of the boundary, S. We will concentrate on functionals defined as time-averaged, integrated quantities on the solid surface,

$$\mathcal{J} = \frac{1}{T} \int_{t_o}^{t_f} \int_S j_S \, ds \, dt, \tag{5}$$

where j_S is a time-dependent scalar function defined at each point on S.

Therefore, the goal is to compute the variation, or change, of Eqn. 5 caused by arbitrary but small (and multiple) deformations of S and to use this information to drive our geometric changes in order to find an optimal shape for the design surface, S. This leads directly to a gradient-based optimization framework. The shape deformations applied to S will be infinitesimal in nature and can be described mathematically by

$$S' = \{\vec{x} + \delta S(\vec{x})\vec{n}_S(\vec{x}), \ \vec{x} \in S\}, \tag{6}$$

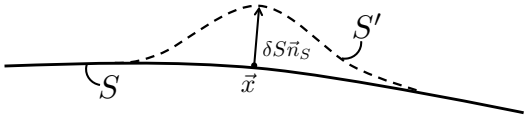

Figure 2. An infinitesimal shape deformation in the local surface normal direction.

where S has been deformed to a new surface S' by applying an infinitesimal profile deformation, δS, in the local normal direction, $\vec{n}_S$, at a point, $\vec{x}$, on the surface, as shown in Fig. 2.

Surface shape deformations will result in variations of the pressure distribution along the surface, so we will focus on pressure-based functionals with the form

$$j_S = \vec{d} \cdot (p\vec{n}_S). \tag{7}$$

The vector $\vec{d}$ is the force projection vector, and it is an arbitrary, constant vector which can be chosen to relate the pressure, p, at the surface to a desired quantity of interest. For aerodynamic applications, likely candidates are

$$\vec{d} = \begin{cases} \left(\frac{1}{C_\infty}\right)(\cos\,\alpha\,\cos\,\beta, \sin\,\alpha\,\cos\,\beta, \sin\,\beta), & C_D \quad \text{Drag coefficient} \\ \left(\frac{1}{C_\infty}\right)(-\sin\,\alpha, \cos\,\alpha, 0), & C_L \quad \text{Lift coefficient} \\ \left(\frac{1}{C_\infty}\right)(-\sin\,\beta\,\cos\,\alpha, -\sin\,\beta\,\sin\,\alpha, \cos\,\beta), & C_{SF} \quad \text{Side-force coefficient} \\ \left(\frac{1}{C_\infty C_D}\right)(-\sin\alpha - \frac{C_L}{C_D}\cos\alpha\cos\beta, -\frac{C_L}{C_D}\sin\beta, \cos\alpha - \frac{C_L}{C_D}\sin\alpha\cos\beta), & \frac{C_L}{C_D} \quad \text{L/D} \end{cases} \tag{8}$$

where $C_\infty = \frac{1}{2}v_\infty^2 \rho_\infty A_z$, v_∞ is the freestream velocity, ρ_∞ is the freestream density, and A_z is the reference area. In practice for a three-dimensional surface, all positive components of the normal surface vectors in the z-direction can be summed in order to calculate the projection A_z. A pre-specified reference area can also be used in a similar fashion, and this is an established procedure in applied aerodynamics.

The minimization of Eqn. 5 can be considered a problem of optimal control whereby the behavior of the governing flow equation system is controlled by the shape of S with deformations of the surface acting as the control input. Mathematically, the PDE-constrained optimization problem can be formulated as follows:

$$\begin{aligned} &\textbf{Minimize} \quad \mathcal{J} = \tfrac{1}{T}\textstyle\int_{t_o}^{t_f}\!\int_S \vec{d}\cdot(p\vec{n}_S)\,ds\,dt \\ &\textbf{such that} \quad \mathcal{R}(U) = 0 \end{aligned} \tag{9}$$

Following the adjoint approach to optimal design, Eqn. 9 can be transformed into an unconstrained optimization problem by adding the inner product of an unsteady adjoint variable vector, Ψ, and the governing equations integrated over the domain (space and time) to form the Lagrangian:

$$\mathcal{J} = \frac{1}{T}\int_{t_o}^{t_f}\!\int_S \vec{d}\cdot(p\vec{n}_S)\,ds\,dt + \frac{1}{T}\int_{t_o}^{t_f}\!\int_\Omega \Psi^T\mathcal{R}(U)\,d\Omega\,dt, \tag{10}$$

where we have introduced the adjoint variables, which operate as Lagrange multipliers and are defined as

$$\Psi = \begin{Bmatrix} \psi_\rho \\ \psi_{\rho u} \\ \psi_{\rho v} \\ \psi_{\rho w} \\ \psi_{\rho E} \end{Bmatrix} = \begin{Bmatrix} \psi_\rho \\ \vec{\varphi} \\ \psi_{\rho E} \end{Bmatrix}. \tag{11}$$

Note that because the flow equations must be satisfied in the domain ($\mathcal{R}(U) = 0$), Eqn. 5 and Eqn. 10 are equivalent. To find the gradient information needed to minimize the objective function, we take the first variation of Eqn. 10 with respect to small perturbations of the surface shape:

$$\delta\mathcal{J} = \frac{1}{T}\int_{t_o}^{t_f}\!\int_S (\vec{d}\cdot\nabla p)\delta S\,ds\,dt + \frac{1}{T}\int_{t_o}^{t_f}\!\int_S (\vec{d}\cdot\vec{n}_S)\delta p\,ds\,dt + \frac{1}{T}\int_{t_o}^{t_f}\!\int_\Omega \Psi^T\delta\mathcal{R}(U)\,d\Omega\,dt. \tag{12}$$

It is important to note that the first two terms of Eqn. 12 are found by using a result from previous work by the second author [7] based on differential geometry formulas, and this is a key feature differentiating the current formulation from other adjoint approaches. The third term of Eqn. 12 can be expanded by including the linearized version of the governing equations with respect to the small perturbations of the design surface

(which induce perturbations in U),

$$\begin{aligned}\delta\mathcal{R}(U) &= \delta\left[\frac{\partial U}{\partial t} + \nabla\cdot\vec{F} - \nabla\cdot(U\otimes\vec{u}_b)\right] \\ &= \frac{\partial}{\partial t}(\delta U) + \nabla\cdot\left(\frac{\partial\vec{F}}{\partial U}\delta U\right) - \nabla\cdot\left[\frac{\partial(U\otimes\vec{u}_b)}{\partial U}\delta U\right] \\ &= \frac{\partial}{\partial t}(\delta U) + \nabla\cdot\left(\vec{A} - \bar{\bar{I}}\vec{u}_b\right)\delta U, \end{aligned} \tag{13}$$

along with the linearized form of the boundary condition at the surface,

$$\delta\vec{v}\cdot\vec{n}_S = -(\vec{v}-\vec{u}_b)\cdot\delta\vec{n}_S - \partial_n(\vec{v}-\vec{u}_b)\cdot\vec{n}_S\delta S, \tag{14}$$

where $\vec{A}$ is the Jacobian of $\vec{F}$ using conservative variables, $\frac{\partial\vec{F}}{\partial U}$. In the first line of Eqn. 13, the terms involving the grid velocity have been separated from the traditional Euler fluxes. Eqn. 13 can now be introduced into Eqn. 12 to produce

$$\begin{aligned}\delta\mathcal{J} = \frac{1}{T}\int_{t_o}^{t_f}\int_S(\vec{d}\cdot\nabla p)\delta S\,ds\,dt + \frac{1}{T}\int_{t_o}^{t_f}\int_S(\vec{d}\cdot\vec{n}_S)\delta p\,ds\,dt + \frac{1}{T}\int_{t_o}^{t_f}\int_\Omega\Psi^T\frac{\partial}{\partial t}(\delta U)\,d\Omega\,dt \\ + \frac{1}{T}\int_{t_o}^{t_f}\int_\Omega\Psi^T\nabla\cdot\left(\vec{A}-\bar{\bar{I}}\vec{u}_b\right)\delta U\,d\Omega\,dt.\end{aligned} \tag{15}$$

By removing any dependence on variations of the flow variables (δp in this case), the variation of the objective function for multiple surface deformations can be found *without* the need for multiple flow solutions. This results in a computationally efficient method for aerodynamic shape design within a large design space, as the computational cost no longer depends on the number of design variables. We now perform manipulations to remove this dependence. After changing the order of integration, integrating the third term of Eqn. 15 by parts gives

$$\int_\Omega\int_{t_o}^{t_f}\Psi^T\frac{\partial}{\partial t}(\delta U)\,dt\,d\Omega = \int_\Omega\left[\Psi^T\delta U\right]_{t_o}^{t_f}d\Omega - \int_\Omega\int_{t_o}^{t_f}\frac{\partial\Psi^T}{\partial t}\delta U\,dt\,d\Omega. \tag{16}$$

A zero-valued initial condition for the adjoint variables can be imposed, and assuming an unsteady flow with periodic behavior, the first term on the right hand side of Eqn. 16 can be eliminated with the following temporal conditions (the cost function does not depend on t_f):

$$\Psi(\vec{x},t_o) = 0, \tag{17}$$

$$\Psi(\vec{x},t_f) = 0. \tag{18}$$

Now, integrating the fourth term of Eqn. 15 by parts yields

$$\int_{t_o}^{t_f}\int_\Omega\Psi^T\nabla\cdot\left(\vec{A}-\bar{\bar{I}}\vec{u}_b\right)\delta U\,d\Omega\,dt = \int_{t_o}^{t_f}\int_\Omega\nabla\cdot\left[\Psi^T\left(\vec{A}-\bar{\bar{I}}\vec{u}_b\right)\delta U\right]d\Omega\,dt - \int_{t_o}^{t_f}\int_\Omega\nabla\Psi^T\cdot\left(\vec{A}-\bar{\bar{I}}\vec{u}_b\right)\delta U d\Omega\,dt, \tag{19}$$

and applying the divergence theorem to the first term on the right hand side of Eqn. 19, assuming a smooth solution, gives

$$\begin{aligned}\int_{t_o}^{t_f}\int_\Omega\Psi^T\nabla\cdot\left(\vec{A}-\bar{\bar{I}}\vec{u}_b\right)\delta U\,d\Omega\,dt = \int_{t_o}^{t_f}\int_S\Psi^T\left(\vec{A}-\bar{\bar{I}}\vec{u}_b\right)\cdot\vec{n}_S\;\delta U ds\,dt + \int_{t_o}^{t_f}\int_{\Gamma_\infty}\Psi^T\left(\vec{A}-\bar{\bar{I}}\vec{u}_b\right)\cdot\vec{n}_S\;\delta U ds\,dt \\ - \int_{t_o}^{t_f}\int_\Omega\nabla\Psi^T\cdot\left(\vec{A}-\bar{\bar{I}}\vec{u}_b\right)\delta U d\Omega\,dt.\end{aligned} \tag{20}$$

With the appropriate choice of characteristic-based boundary conditions, the integral over the far-field boundary can be forced to vanish. Combining and rearranging the results from Eqns. 15, 16 (after reversing the

order of integration again), 17, 18 & 20 yields an intermediate expression for the variation of the cost function,

$$\delta\mathcal{J} = \frac{1}{T}\int_{t_o}^{t_f}\int_S (\vec{d}\cdot\nabla p)\delta S\, ds\, dt + \frac{1}{T}\int_{t_o}^{t_f}\int_S (\vec{d}\cdot\vec{n}_S)\delta p\, ds\, dt + \frac{1}{T}\int_{t_o}^{t_f}\int_S \Psi^T\left(\vec{A}-\bar{\bar{I}}\vec{u}_b\right)\cdot\vec{n}_S\ \delta U ds\, dt$$
$$- \frac{1}{T}\int_{t_o}^{t_f}\int_\Omega \left[\frac{\partial\Psi^T}{\partial t} + \nabla\Psi^T\cdot\left(\vec{A}-\bar{\bar{I}}\vec{u}_b\right)\right]\delta U\, d\Omega\, dt. \tag{21}$$

The surface integral in the third term on the right hand side of Eqn. 21 can be evaluated given our knowledge of $\vec{A}$, $\vec{u}_b$, the wall boundary condition, and the linearized wall boundary condition in Eqn. 14. By leveraging previous derivation by the authors [8] with some small modifications (including time integration), it can be shown that evaluating the surface integral and rearranging the variation of the functional gives

$$\delta\mathcal{J} = \frac{1}{T}\int_{t_o}^{t_f}\int_S \left[\vec{d}\cdot\nabla p + (\nabla\cdot\vec{v})\vartheta + (\vec{v}-\vec{u}_b)\cdot\nabla(\vartheta)\right]\delta S\, ds\, dt$$
$$+ \frac{1}{T}\int_{t_o}^{t_f}\int_S \left[\vec{d}\cdot\vec{n}_S - \vec{n}_S\cdot\vec{\varphi} - \psi_{\rho E}(\vec{v}\cdot\vec{n}_S)\right]\delta p\, ds\, dt - \frac{1}{T}\int_{t_o}^{t_f}\int_\Omega \left[\frac{\partial\Psi^T}{\partial t} + \nabla\Psi^T\cdot\left(\vec{A}-\bar{\bar{I}}\vec{u}_b\right)\right]\delta U\, d\Omega\, dt, \tag{22}$$

where $\vartheta = \rho\psi_\rho + \rho\vec{v}\cdot\vec{\varphi} + \rho H\psi_{\rho E}$. Finally, by satisfying the system of PDEs commonly referred to as the adjoint equations along with the admissible adjoint boundary condition that eliminates the dependence on the fluid flow variations (δp), both the second and third terms on the right hand side of Eqn. 22 can be eliminated:

$$\begin{cases} \frac{\partial\Psi}{\partial t} + \left(\vec{A}-\bar{\bar{I}}\vec{u}_b\right)^T\cdot\nabla\Psi = 0, & \text{in } \Omega, \quad t_o \le t \le t_f \\ \vec{n}_S\cdot\vec{\varphi} = \vec{d}\cdot\vec{n}_S - \psi_{\rho E}(\vec{v}\cdot\vec{n}_S), & \text{on } S, \quad t_o \le t \le t_f \end{cases} \tag{23}$$

where a transpose operation has been performed on the adjoint equations. The variation of the objective function becomes

$$\delta\mathcal{J} = \frac{1}{T}\int_{t_o}^{t_f}\int_S \left[\vec{d}\cdot\nabla p + (\nabla\cdot\vec{v})\vartheta + (\vec{v}-\vec{u}_b)\cdot\nabla(\vartheta)\right]\delta S\, ds\, dt = \frac{1}{T}\int_{t_o}^{t_f}\int_S \frac{\partial\mathcal{J}}{\partial S}\delta S\, ds\, dt, \tag{24}$$

where $\frac{\partial\mathcal{J}}{\partial S} = \vec{d}\cdot\nabla p + (\nabla\cdot\vec{v})\vartheta + (\vec{v}-\vec{u}_b)\cdot\nabla(\vartheta)$ is what we call the *surface sensitivity*. The surface sensitivity provides a measure of the variation of the objective function with respect to infinitesimal variations of the surface shape in the direction of the local surface normal. With each physical time step, this value is computed at every surface node of the numerical grid with negligible computational cost. Note that the final expression for the variation involves only a surface integral and has no dependence on the volume mesh.

III. Governing Wave and Adjoint Equations for Aeroacoustics

In this section we detail the governing equation for aerodynamically generated sound and also present a new continuous adjoint formulation for the control of noise.

A. Description of the Aeroacoustic Problem

We are interested in predicting and controlling the noise generated by aerodynamic surfaces that might be in motion. For aeroacoustic problems, perturbations in density, ρ' where $\rho'(\vec{x},t) = \rho(\vec{x},t) - \rho_\infty$, form the longitudinal waves that are perceived as sound. Consider the aerodynamic body in Fig. 3 which is immersed in an unbounded volume of fluid, Ω. A fictitious, near-field control surface, Γ_{nf}, is placed near the body, and the fluid domain is therefore divided into two regions, labeled Ω_1 and Ω_2. As a mathematical convenience, we define the shape of Γ_{nf} by a function, $f = 0$, such that $f < 0$ inside the body and $f > 0$ outside the body. We also assume that $\nabla(f)$ is in the direction of the outward normal, such that $\nabla(f) = \vec{n}_{\Gamma_{nf}}|\nabla(f)|$. Furthermore, Γ_{nf} can be in motion with arbitrary boundary velocity, $\vec{u}_b$.

Following the derivation by Ffowcs Williams and Hawkings [9], generalized formulations for the continuity and momentum equation in an unbounded fluid can be obtained:

$$\begin{aligned} &\frac{\partial\rho}{\partial t} + \nabla\cdot(\rho\vec{v}) = [\rho(\vec{v}-\vec{u}_b)]_{(1)}^{(2)}\cdot\nabla(f)\delta(f) && \text{in } \Omega, \\ &\frac{\partial}{\partial t}(\rho\vec{v}) + \nabla\cdot(\rho\vec{v}\otimes\vec{v} + \bar{\bar{I}}p) = \left[\rho\vec{v}\otimes(\vec{v}-\vec{u}_b) + \bar{\bar{I}}p\right]_{(1)}^{(2)}\cdot\nabla(f)\delta(f) && \text{in } \Omega, \end{aligned} \tag{25}$$

where, in this case, $\delta(f)$ is the Dirac delta function involving the near-field surface and *not* the variation of f. The nomenclature $[\,]_{(1)}^{(2)}$ represents the jump between regions Ω_2 and Ω_1. Eqn. 25 contains general forms for an unbounded fluid that are valid everywhere in space, and that if there are no discontinuities, the right hand sides disappear and the usual conservation equations are recovered. The terms appearing on the right hand sides can be thought of as sources concentrated at the surface, Γ_{nf}, which are required to maintain conservation for the unbounded fluid.

We now replace the volume within Ω_1 by fluid at a mean state with density ρ_∞ and pressure p_∞ and evaluate the source terms above. Since the mean stress state on both sides of Γ_{nf} is the same, the term $\bar{\bar{I}}p_\infty$ would vanish during the subtraction involved with the source term in the generalized momentum equation of Eqn. 25. Therefore, it will be replaced by the term p' which represents the fluctuating components of the stress tensor. If Γ_{nf} is made coincident with the solid aerodynamic body, one can obtain the inhomogeneous wave equation known as the classic Ffowcs Williams-Hawkings (FW-H) equation. However, in our case, Γ_{nf} is not coincident with the body, and fluid may flow through this fictitious near-field, as there is no solid body to enforce a no-penetration condition. By eliminating $\rho\vec{v}$ from the generalized mass and momentum equations, the permeable surface version of the FW-H equation can be formulated as

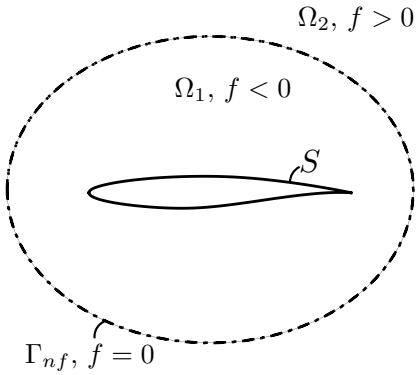

Figure 3. Control surface (dashed line), Γ_{nf}, enclosing the physical body surface, S. The fictitious control surface is defined mathematically by a function, $f = 0$.

$$\frac{\partial^2\rho'}{\partial t^2} - c^2\nabla^2\rho' = \frac{\partial}{\partial t}\left\{[\rho(\vec{v}-\vec{u}_b)+\rho_\infty\vec{u}_b]\cdot\nabla(f)\delta(f)\right\} - \nabla\cdot\left\{\left[\rho\vec{v}\otimes(\vec{v}-\vec{u}_b)+\bar{\bar{I}}p'\right]\cdot\nabla(f)\delta(f)\right\} + \nabla^2\mathbb{T} \quad \text{in } \Omega,\ t>0, \tag{26}$$

where c is the constant speed of sound and $\mathbb{T} = \rho\vec{v}\otimes\vec{v} + P - \bar{\bar{I}}a^2\rho'$ is the Lighthill stress tensor that represents the difference between the stress state in the real fluid and that in the acoustic medium. Here we see that the propagation of sound generated by aerodynamic surfaces in arbitrary motion is governed by the wave equation, and the sound generation processes are composed of three types of sources on the right hand side: a mass displacement effect by the surface with monopole character (thickness noise, first term), a surface distribution of dipoles (loading noise, second term), and a distribution of quadrupole noise sources throughout the volume exterior to the surface (third term). For simplicity in further development, the source terms will be lumped together as a single term, $\mathcal{Q}$, giving

$$\frac{\partial^2\rho'}{\partial t^2} - c^2\nabla^2\rho' = \mathcal{Q} \quad \text{in } \Omega,\ t>0. \tag{27}$$

B. Continuous Adjoint Formulation for Controlling Aerodynamically Generated Noise

Consider the mathematical domain depicted by Fig. 4. We are interested in controlling the noise generated by an aerodynamic body that is perceived at a certain permeable observer surface, Γ_{obs}. For now, we will assume that the aerodynamic body can be represented by a distribution of sources, $\mathcal{Q}$, in the domain, Ω, without detailing their formulation. In this manner, we can consider the general problem of controlling wave behavior resulting from an arbitrary distribution of sources, which might have wider applicability to problems in physics and engineering.

One approach for controlling noise is to minimize a measure of the total sound amplitude integrated over the observer surface. A suitable cost function for this problem involving the time-averaged acoustic pressure, or the acoustic density (for linear acoustics, $p' = c^2\rho'$), can be written as

$$\mathcal{I} = \frac{1}{T}\int_{t_o}^{t_f}\int_{\Gamma_{obs}} p'^2\, ds\, dt = \frac{1}{T}\int_{t_o}^{t_f}\int_{\Gamma_{obs}} (c^2\rho')^2\, ds\, dt. \tag{28}$$

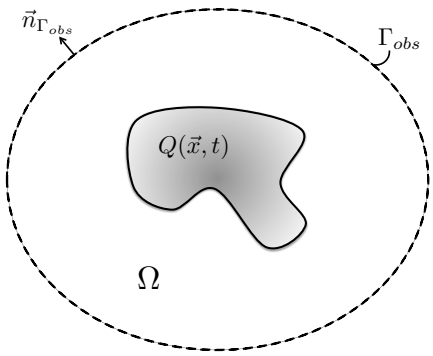

Figure 4. Schematic of the domain, Ω, for the acoustic problem. We are concerned with the noise generated by an arbitrary distribution of sources, $\mathcal{Q}$, observed at a surface, Γ_{obs}.

Other cost functions are possible, such as matching a specified target acoustic signature in time on Γ_{obs}. For instance, this target signature might call for a reduction in the total strength of the noise, or perhaps an adjustment in the frequency content. Controlling the noise requires knowledge of the system, and in our problem, the generation and propagation of aerodynamically generated sound is governed by an inhomogeneous wave equation (FW-H equation):

$$\mathcal{N}(\rho') = \frac{\partial^2 \rho'}{\partial t^2} - c^2 \nabla^2 \rho' - \mathcal{Q} = 0 \ \text{ in } \Omega, \ t_o \leq t \leq t_f, \tag{29}$$

where $\mathcal{Q}$ is the distribution of sources. The sources will act as the input for controlling the noise at the observer surface. In words, we seek to minimize the total noise at Γ_{obs} through changes in the source terms, $\mathcal{Q}$, that generate the sound which is propagated through the domain by the wave equation. Mathematically, the PDE-constrained optimization problem can be formulated as follows:

$$\begin{array}{ll} \textbf{Minimize} & \mathcal{I} = \frac{1}{T}\int_{t_o}^{t_f}\int_{\Gamma_{obs}} (c^2\rho')^2 \, ds \, dt \\ \textbf{such that} & \mathcal{N}(\rho') = 0 \end{array} \tag{30}$$

Again following the adjoint approach to optimal design, Eqn. 30 can be transformed into an unconstrained optimization problem by taking the inner product of an adjoint variable, ϕ, and the governing equation, $\mathcal{N}(\rho')$, to form the Lagrangian:

$$\mathcal{I} = \frac{1}{T}\int_{t_o}^{t_f}\int_{\Gamma_{obs}} (c^2\rho')^2 \, ds \, dt + \frac{1}{T}\int_{t_o}^{t_f}\int_{\Omega} \phi \, \mathcal{N}(\rho') \, d\Omega \, dt. \tag{31}$$

The gradient information needed for minimizing $\mathcal{I}$ can be obtained by taking its first variation with respect to perturbations in the source term,

$$\begin{aligned} \delta\mathcal{I} &= \frac{1}{T}\int_{t_o}^{t_f}\int_{\Gamma_{obs}} 2c^2\rho'\delta\rho' \, ds \, dt + \frac{1}{T}\int_{t_o}^{t_f}\int_{\Omega} \phi \, \delta\mathcal{N}(\rho') \, d\Omega \, dt \\ &= \frac{1}{T}\int_{t_o}^{t_f}\int_{\Gamma_{obs}} 2c^2\rho'\delta\rho' \, ds \, dt + \frac{1}{T}\int_{t_o}^{t_f}\int_{\Omega} \phi \left[\frac{\partial^2}{\partial t^2}(\delta\rho') - c^2\nabla^2(\delta\rho') - \delta Q\right] d\Omega \, dt. \\ &= \frac{1}{T}\int_{t_o}^{t_f}\int_{\Gamma_{obs}} 2c^2\rho'\delta\rho' \, ds \, dt + \frac{1}{T}\int_{t_o}^{t_f}\int_{\Omega} \phi\frac{\partial^2}{\partial t^2}(\delta\rho') \, d\Omega \, dt - \frac{c^2}{T}\int_{t_o}^{t_f}\int_{\Omega} \phi\nabla^2(\delta\rho') \, d\Omega \, dt - \frac{1}{T}\int_{t_o}^{t_f}\int_{\Omega} \phi \, \delta Q \, d\Omega \, dt. \end{aligned} \tag{32}$$

After changing the order of integration, integrating the second term on the right hand side of Eqn. 32 by parts gives

$$\int_{\Omega}\int_{t_o}^{t_f} \phi\frac{\partial^2}{\partial t^2}(\delta\rho') \, dt \, d\Omega = \int_{\Omega}\left[\phi\frac{\partial}{\partial t}(\delta\rho')\right]_{t_o}^{t_f} d\Omega - \int_{\Omega}\int_{t_o}^{t_f} \frac{\partial\phi}{\partial t}\frac{\partial}{\partial t}(\delta\rho') \, dt \, d\Omega, \tag{33}$$

and again integrating the final term of Eqn. 33 by parts results in

$$\int_{\Omega}\int_{t_o}^{t_f} \phi\frac{\partial^2}{\partial t^2}(\delta\rho') \, dt \, d\Omega = \int_{\Omega}\left[\phi\frac{\partial}{\partial t}(\delta\rho')\right]_{t_o}^{t_f} d\Omega - \int_{\Omega}\left[\frac{\partial\phi}{\partial t}\delta\rho'\right]_{t_o}^{t_f} d\Omega + \int_{t_o}^{t_f}\int_{\Omega} \frac{\partial^2\phi}{\partial t^2}\delta\rho' \, d\Omega \, dt, \tag{34}$$

where the order of integration in the final term has been reversed again. Consider now the third term on the right hand side of Eqn. 32. Integrating by parts and using the divergence theorem (assuming a smooth solution) yields

$$\int_{t_o}^{t_f}\int_{\Omega} \phi\nabla^2(\delta\rho') \, d\Omega \, dt = \int_{t_o}^{t_f}\int_{\Gamma_{obs}} \phi\nabla(\delta\rho') \cdot \vec{n}_{\Gamma_{obs}} \, ds \, dt - \int_{t_o}^{t_f}\int_{\Omega} \nabla(\phi) \cdot \nabla(\delta\rho') \, d\Omega \, dt, \tag{35}$$

and integrating the final term of Eqn. 35 by parts and using the divergence theorem a second time results in

$$\int_{t_o}^{t_f}\int_{\Omega} \phi\nabla^2(\delta\rho')\,d\Omega\,dt = \int_{t_o}^{t_f}\int_{\Gamma_{obs}} \phi\nabla(\delta\rho')\cdot\vec{n}_{\Gamma_{obs}}\,ds\,dt - \int_{t_o}^{t_f}\int_{\Gamma_{obs}} \nabla(\phi)\cdot\vec{n}_{\Gamma_{obs}}\delta\rho'\,ds\,dt + \int_{t_o}^{t_f}\int_{\Omega} \nabla^2\phi\ \delta\rho'\,d\Omega\,dt. \tag{36}$$

The first term on the right hand side of Eqn. 36 can be eliminated by adding and subtracting again the second term, or

$$\begin{aligned}
&\int_{t_o}^{t_f}\int_{\Omega} \phi\nabla^2(\delta\rho')\,d\Omega\,dt \\
&\quad= \int_{t_o}^{t_f}\int_{\Gamma_{obs}} [\phi\nabla(\delta\rho') + \nabla(\phi)\delta\rho']\cdot\vec{n}_{\Gamma_{obs}}\,ds\,dt - 2\int_{t_o}^{t_f}\int_{\Gamma_{obs}} \nabla(\phi)\cdot\vec{n}_{\Gamma_{obs}}\delta\rho'\,ds\,dt + \int_{t_o}^{t_f}\int_{\Omega} \nabla^2\phi\ \delta\rho'\,d\Omega\,dt \\
&\quad= \int_{t_o}^{t_f}\int_{\Gamma_{obs}} \nabla(\phi\ \delta\rho')\cdot\vec{n}_{\Gamma_{obs}}\,ds\,dt - 2\int_{t_o}^{t_f}\int_{\Gamma_{obs}} \nabla(\phi)\cdot\vec{n}_{\Gamma_{obs}}\delta\rho'\,ds\,dt + \int_{t_o}^{t_f}\int_{\Omega} \nabla^2\phi\ \delta\rho'\,d\Omega\,dt \\
&\quad= -2\int_{t_o}^{t_f}\int_{\Gamma_{obs}} \nabla(\phi)\cdot\vec{n}_{\Gamma_{obs}}\delta\rho'\,ds\,dt + \int_{t_o}^{t_f}\int_{\Omega} \nabla^2\phi\ \delta\rho'\,d\Omega\,dt,
\end{aligned} \tag{37}$$

where, in going from the second to the third line, we have used the mathematical identity that a gradient dotted with the normal and integrated over a closed surface is zero.

After substituting the results from Eqns. 34 & 37 into Eqn. 32 and rearranging terms based on integral type, the variation of the cost function becomes

$$\begin{aligned}
\delta\mathcal{I} = \frac{1}{T}\int_{t_o}^{t_f}\int_{\Gamma_{obs}} \left[2c^2\rho' + 2c^2\nabla(\phi)\cdot\vec{n}_{\Gamma_{obs}}\right]\delta\rho'\,ds\,dt + \frac{1}{T}\int_{\Omega}\left[\phi\frac{\partial}{\partial t}(\delta\rho')\right]_{t_o}^{t_f} d\Omega - \frac{1}{T}\int_{\Omega}\left[\frac{\partial\phi}{\partial t}\delta\rho'\right]_{t_o}^{t_f} d\Omega \\
+ \frac{1}{T}\int_{t_o}^{t_f}\int_{\Omega}\left[\frac{\partial^2\phi}{\partial t^2} - c^2\nabla^2\phi\right]\delta\rho'\,d\Omega\,dt - \frac{1}{T}\int_{t_o}^{t_f}\int_{\Omega}\phi\ \delta\mathcal{Q}\,d\Omega\,dt.
\end{aligned} \tag{38}$$

Many of the terms in Eqn. 38 can be eliminated by satisfying the adjoint wave equation with the permissible boundary and temporal conditions,

$$\begin{cases}
\frac{\partial^2\phi}{\partial t^2} - c^2\nabla^2\phi = 0, & \text{in } \Omega, \quad t_o \le t \le t_f \\
\partial_n\phi = -\rho', & \text{on } \Gamma_{obs}, \quad t_o \le t \le t_f \\
\phi(\vec{x}, t_o) = 0, \frac{\partial\phi(\vec{x},t_o)}{\partial t} = 0. & \text{in } \Omega
\end{cases} \tag{39}$$

Note that the wave equation is self-adjoint, meaning that the corresponding adjoint equation is again the wave equation. As with the adjoint flow equations, if there is periodic behavior (the cost function does not depend on t_f), then the second and third integrals on the right hand side can be completely eliminated by imposing $\phi(\vec{x}, t_f) = 0$ and $\frac{\partial\phi(\vec{x},t_f)}{\partial t} = 0$. The final result is a simple expression for the variation of the cost function,

$$\delta\mathcal{I} = -\frac{1}{T}\int_{t_o}^{t_f}\int_{\Omega}\phi\ \delta\mathcal{Q}\,d\Omega\,dt. \tag{40}$$

While the result in Eqn. 40 is general, we will limit the design space to a particular form for the sources, $\mathcal{Q}$. More specifically, the sources will have the form of those appearing in the FW-H equation, or $\mathcal{Q} = \mathcal{Q}(U(\vec{x},t))\delta(f)$.

IV. Coupling Strategy for the Aerodynamic and Aeroacoustic MDO Problem

We are interested in finding the sensitivity of the perceived noise at Γ_{obs} due to shape changes on an aerodynamic body of interest, S. Because the functional is defined away from the body surface in the CAA domain, we will refer to these as *remote sensitivities*. CFD is performed in the region near the body, and the CFD domain is overlapped with a larger acoustic domain that reaches some observer surface, Γ_{obs}. A schematic of this domain architecture is shown in Fig. 5. The link between the two problems occurs at the

near-field interface, Γ_{nf}, where the CFD solution is used as input for the CAA method in the form of source terms for the wave equation. In terms of the coupled analysis problem, any perturbations to the shape of S will cause variations that propagate through the CFD solution, are transferred to the wave solver through the source terms at Γ_{nf}, and ultimately propagate through the wave solution where they result in a change in the total integrated noise at Γ_{obs}.

How then does a designer obtain sensitivities for a remote objective with respect to surface shape changes in order to improve a design, or in this case, to reduce the noise? Following the coupling strategy for finding remote sensitivities by Alonso, et al. [10], the flow and acoustic adjoint formulations can be linked at Γ_{nf} by defining a new cost function for the aerodynamic problem:

$$\mathcal{J} = -\frac{1}{T}\int_{t_o}^{t_f}\int_{\Omega} \phi \ \mathcal{Q}\, d\Omega\, dt, \tag{41}$$

such that the first variation is equivalent to that of the aeroacoustic adjoint formulation above for reducing noise, or

$$\delta\mathcal{J} = -\frac{1}{T}\int_{t_o}^{t_f}\int_{\Omega} \phi\ \frac{\partial \mathcal{Q}}{\partial U}\delta U\, d\Omega\, dt. \tag{42}$$

Recalling the Dirac delta functions that appear in $\mathcal{Q}$ for our particular problem, only an integral over the near-field surface will remain, or

$$\delta\mathcal{J} = -\frac{1}{T}\int_{t_o}^{t_f}\int_{\Gamma_{nf}} \phi\ \frac{\partial \mathcal{Q}}{\partial U}\delta U\, ds\, dt. \tag{43}$$

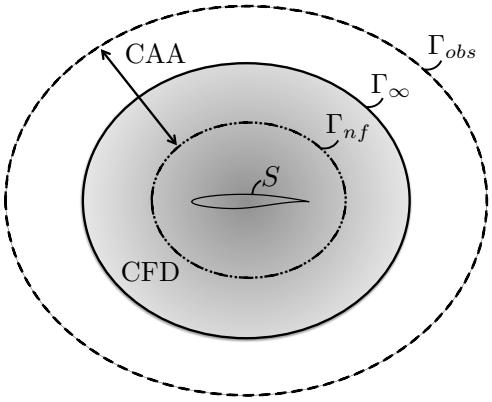

Figure 5. Notional schematic of the coupled aerodynamic and aeroacoustic domains. The CFD domain may overlap or be a subset of the CAA domain. The resulting CFD flow state at the near-field surface, Γ_{nf}, becomes the input for the wave equation source terms in the CAA solver.

By construction, we are solving the noise minimization problem from the aeroacoustic adjoint formulation expressed within the aerodynamic domain. Again following the adjoint approach, Eqn. 43 can be augmented with the variation of the flow equations as

$$\delta\mathcal{J} = -\frac{1}{T}\int_{t_o}^{t_f}\int_{\Gamma_{nf}} \phi\ \frac{\partial \mathcal{Q}}{\partial U}\delta U\, ds\, dt + \frac{1}{T}\int_{t_o}^{t_f}\int_{\Omega} \Psi^T \delta\mathcal{R}(U)\, d\Omega\, dt, \tag{44}$$

and following the same procedure for arriving at Eqn. 21 gives

$$\begin{aligned}\delta\mathcal{J} = &-\frac{1}{T}\int_{t_o}^{t_f}\int_{\Gamma_{nf}} \phi\ \frac{\partial \mathcal{Q}}{\partial U}\delta U\, ds\, dt + \frac{1}{T}\int_{t_o}^{t_f}\int_{S} \Psi^T\left(\vec{A} - \bar{\bar{I}}\vec{u}_b\right)\cdot\vec{n}_S\ \delta U ds\, dt \\ &+ \frac{1}{T}\int_{t_o}^{t_f}\int_{\Gamma_{nf}} \Psi^T\left(\vec{A} - \bar{\bar{I}}\vec{u}_b\right)\cdot\vec{n}_{\Gamma_{nf}}\ \delta U ds\, dt - \frac{1}{T}\int_{t_o}^{t_f}\int_{\Omega}\left[\frac{\partial \Psi^T}{\partial t} + \nabla\Psi^T\cdot\left(\vec{A} - \bar{\bar{I}}\vec{u}_b\right)\right]\delta U\, d\Omega\, dt.\end{aligned} \tag{45}$$

Certain integrals can again be eliminated to find an expression for the surface sensitivity, $\frac{\partial J}{\partial S}$, involving only the adjoint variables and other known quantities, and in particular, a new boundary condition for the flow adjoint problem has emerged at the near-field surface. This admissible boundary condition for removing any contributions involving integrals on Γ_{nf} (first and third terms of Eqn. 45) can be expressed as

$$\Psi^T\left(\vec{A} - \bar{\bar{I}}\vec{u}_b\right)\cdot\vec{n}_{\Gamma_{nf}} = \phi\ \frac{\partial \mathcal{Q}}{\partial U}\ \text{ on } \Gamma_{nf},\ t_o \le t \le t_f. \tag{46}$$

Eqn. 46 requires the solution of a small system of equations at each node on Γ_{nf} with every physical time step, and clearly it is also a requirement that this system be solvable. The new condition relates the two adjoint formulations through the same source terms that couple the direct analysis problem. However, now it is their Jacobian in conservative variables, $\frac{\partial \mathcal{Q}}{\partial U}$, that provides the coupling mechanism.

Again, the expression chosen for δJ is equivalent to the variation of the aeroacoustic cost function above, δI, so the new boundary condition represents the coupling of the two adjoint problems. The acoustic adjoint

solution, ϕ, will now be required on Γ_{nf} at each time instance when solving the flow adjoint, and this is a reversal of the one-way coupling from the analysis problem. Another key difference between the flow adjoint derivation above and the coupled formulation described here is that there is no longer a dependence on the force projection vector, $\vec{d}$. This is due to the choice of functional, as we are no longer specifically interested in the pressure on S when controlling noise. Instead, $\vec{d} = \vec{0}$, and the flow adjoint problem becomes,

$$\begin{cases} \frac{\partial \Psi}{\partial t} + \left(\vec{A} - \bar{\bar{I}}\vec{u}_b\right)^T \cdot \nabla \Psi = 0, & \text{in } \Omega, \quad t_o \leq t \leq t_f \\ \vec{n}_S \cdot \vec{\varphi} = -\psi_{\rho E}(\vec{v} \cdot \vec{n}_S), & \text{on } S, \quad t_o \leq t \leq t_f \end{cases} \tag{47}$$

resulting in the following expression for the surface sensitivity to noise at a remote observer location:

$$\delta \mathcal{J} = \frac{1}{T} \int_{t_o}^{t_f} \int_S \left[(\nabla \cdot \vec{v})\vartheta + (\vec{v} - \vec{u}_b) \cdot \nabla(\vartheta) \right] \delta S \, ds \, dt = \frac{1}{T} \int_{t_o}^{t_f} \int_S \frac{\partial \mathcal{J}}{\partial S} \delta S \, ds \, dt. \tag{48}$$

V. Numerical Implementation

A. Numerical discretization of the compressible Euler equations

Solution procedures for both the compressible Euler equations and the corresponding adjoint equations were implemented within the SU^2 software suite (**S**tanford **U**niversity **U**nstructured). This collection of C++ codes is built specifically for PDE analysis and PDE-constrained optimization on unstructured meshes, and it is particularly well-suited for aerodynamic shape design. Modules for performing direct and adjoint flow solutions, acquiring gradient information by projecting surface sensitivities into the design space, and deforming meshes are included in the suite, amongst others. Scripts written in the Python programming language are also used to automate execution of the SU^2 suite components, especially for performing shape optimization.

Both the direct and adjoint flow problems are solved using a Finite Volume Method (FVM) formulation with an edge-based structure. The code is fully parallel and takes advantage of an agglomeration multigrid approach for convergence acceleration. The unsteady Euler equations are spatially discretized using a central scheme with JST-type artificial dissipation [11], and the adjoint equations use a slightly modified JST scheme. Time integration is handled by a second-order accurate dual-time stepping approach for both the analysis and adjoint problems [12]. Note that solving the adjoint equations requires integration in reverse time. This is accomplished by storing the solution data at time steps during the analysis problem and then retrieving the data in reverse order while time-marching the adjoint equations.

B. Numerical discretization of the wave equation

In this section a basic introduction to the Finite Element Method (FEM) technique is presented which has also been implemented within the SU^2 software suite. The final objective is the numerical discretization of the wave equation with a source term $\mathcal{Q} = \mathcal{Q}(\vec{x}, t)$.

$$\frac{\partial^2 V}{\partial t^2} - c^2 \nabla^2 V = \mathcal{Q}, \text{ in } \Omega, \ t > 0 \tag{49}$$

using Dirichlet and Neumann boundary conditions.

Finite-element methods of solution are based upon approximations to a variational formulation of the problem. A variational formulation requires the introduction of a space of trial functions, $\mathcal{T} = \{V(t, \vec{x})\}$, and a space of weighting functions $\mathcal{W} = \{W(t, \vec{x})\}$. The problem consists in finding $V(t, \vec{x})$ in $\mathcal{T}$, satisfying the problem boundary conditions, such that

$$\int_\Omega W^T \left(\frac{\partial^2 V}{\partial t^2} - c^2 \nabla^2 V - \mathcal{Q} \right) d\Omega = 0 \tag{50}$$

To produce an approximate solution to the variational problem, a grid of finite elements is constructed on the domain Ω. It will be assumed that the discretization employs p nodes. Finite-dimensional subspaces

$\mathcal{T}^{(p)}$ and $\mathcal{W}^{(p)}$ of the trial and weighting function spaces, respectively, are defined by

$$\mathcal{T}^{(p)} = \left\{ V^{(p)}(t,\vec{x}) \,|\, V^{(p)} = \sum_{J=1}^{p} V_J(t) N_J(\vec{x}) \right\}, \tag{51}$$

$$\mathcal{W}^{(p)} = \left\{ W^{(p)}(t,\vec{x}) \,|\, W^{(p)} = \sum_{J=1}^{p} a_J(t) N_J(\vec{x}) \right\}, \tag{52}$$

where $V_J(t)$ is the value of $V^{(p)}$ at node J and time t. On the other hand, $a_1, a_2, \ldots, a_p$ are constant, and $N_J(\vec{x})$ is the piecewise linear trial function associated with node J. We now apply the finite element approximation by discretizing the domain of the problem into elements and introducing functions which interpolate the solution over nodes that compose the elements. The Galerkin approximation is determined by applying the variational formulation of Eqn. 50 in the following form: find $V^{(p)}$ in $\mathcal{T}^{(p)}$, satisfying the problem boundary conditions, such that

$$\int_\Omega N_I^T \left(\frac{\partial^2 V}{\partial t^2} - c^2 \nabla^2 V \right) d\Omega = \int_\Omega N_I^T \mathcal{Q} \, d\Omega, \tag{53}$$

for $I = 1, 2, ..., p$. The form assumed for $V^{(p)}$ in Eqn. 51 can now be inserted into the left hand side of Eqn. 53 and the result can be written as

$$\int_\Omega N_I^T \left(\sum_{J=1}^{p} \frac{\partial^2 V_J}{\partial t^2} N_J - c^2 \sum_{J=1}^{p} V_J \nabla^2 N_J \right) d\Omega = \int_\Omega N_I^T \mathcal{Q} \, d\Omega. \tag{54}$$

Rearranging terms we obtain

$$\sum_{J=1}^{p} \frac{\partial^2 V_J}{\partial t^2} \left(\int_\Omega N_I^T N_J \, d\Omega \right) - \sum_{J=1}^{p} c^2 V_J \left(\int_\Omega N_I^T \nabla^2 N_J \, d\Omega \right) = \int_\Omega N_I^T \mathcal{Q} \, d\Omega, \tag{55}$$

and applying the divergence theorem gives

$$\sum_{J=1}^{p} \frac{\partial^2 V_J}{\partial t^2} \left(\int_\Omega N_I^T N_J \, d\Omega \right) - \sum_{J=1}^{p} c^2 V_J \left(\int_\Gamma N_I^T \left(\nabla N_J \cdot \vec{\nu} \right) d\Gamma - \int_\Omega \nabla N_I^T \cdot \nabla N_J \, d\Omega \right) = \int_\Omega N_I^T \mathcal{Q} \, d\Omega, \tag{56}$$

where the boundary integral disappears unless we are computing a boundary element with non-homogeneous Neumann conditions (I is an exterior node). The result at a typical interior node I is

$$\sum_{E \in I} \sum_{J \in E} \frac{\partial^2 V_J}{\partial t^2} \left(\int_{\Omega_E} N_I^T N_J \, d\Omega \right) + \sum_{E \in I} \sum_{J \in E} c^2 V_J \left(\int_{\Omega_E} \nabla N_I^T \cdot \nabla N_J \, d\Omega \right) = \sum_{E \in I} \sum_{J \in E} \mathcal{Q}_J \left(\int_{\Omega_E} N_I^T N_J \, d\Omega \right), \tag{57}$$

where the first summation extends over the elements E in the numerical grid which contain node I and the second summation extends over nodes J of the elements E. Ω_E is the portion of Ω which is represented by element E. Note that the field variables $\mathcal{Q}$ are interpolated from the nodal variables by using the shape functions.

Finally, the time discretization is performed using a second order formula,

$$\frac{\partial^2 W}{\partial t^2} = \frac{2u^{n+1} - 5u^{n-1} + 4u^{n-1} - u^{n-2}}{\Delta t^2}, \tag{58}$$

or by splitting the original equation into two partial differential equations where only a first order time derivative appears:

$$\frac{\partial W}{\partial t} = AW + g \text{ where, } W = \begin{bmatrix} V \\ U \end{bmatrix}, A = \begin{bmatrix} 0 & I \\ c^2 \nabla^2 & 0 \end{bmatrix}, g = \begin{bmatrix} 0 \\ \mathcal{Q} \end{bmatrix}. \tag{59}$$

Due to the self-adjoint nature of the wave equation, the same numerical solver can be used for both the analysis and adjoint wave problems. Again, however, the adjoint problem requires integration in reverse time.

C. Design Variable Definition and Mesh Deformation

The above coupled-adjoint methodology offers a way to compute the variation of an objective function with respect to infinitesimal shape deformations in the direction of the local normal at points on the design surface. While it is possible to use each surface node in the computational mesh as a design variable capable of deformation, this approach is not often pursued. A more practical choice involves computing the surface sensitivities at each mesh node on the design surface and then projecting this information into a design space made up of a smaller set of design variables (possibly a complete basis). The procedure for computing the surface sensitivities can be used repeatedly in a gradient-based optimization framework in order to march the surface shape toward an optimum through gradient projection and mesh deformation.

In the two-dimensional airfoil calculations that follow, Hicks-Henne bump functions were employed [13] which can be added to the original airfoil geometry to modify the shape. The Hicks-Henne function with maximum at point x_n is given by

$$f_n(x) = \sin^3(\pi x^{e_n}),\ e_n = \frac{\log(0.5)}{\log(x_n)},\ x \in [0,1], \tag{60}$$

so that the total deformation of the surface can be computed as $\Delta y = \sum_{n=1}^{N} \delta_n f_n(x)$, with N being the number of bump functions and δ_n the design variable step. These functions are applied separately to the upper and lower surfaces. After applying the bump functions to recover a new surface shape with each design cycle, a spring analogy method is used to deform the volume mesh around the airfoil [14].

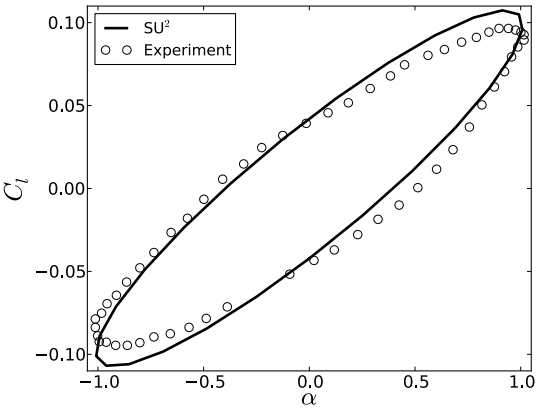

(a) Comparison of lift coefficient versus angle of attack in degrees between SU^2 and experiment.

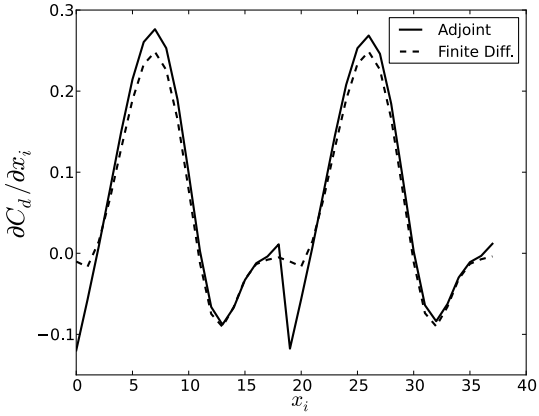

(b) Comparison of gradients obtained via the time-accurate continuous adjoint and finite differencing for 38 Hicks-Henne bump functions.

Figure 6. Numerical results for a pitching NACA 64A010 in transonic flow.

VI. Numerical Results

A. Verification and Validation of the Unsteady Flow and Adjoint Equations

For validating our implementation of the unsteady Euler equations in ALE form, a comparison was made against the well-known CT6 data set of Davis [15]. The physical experiment measured the unsteady performance for the NACA 64A010 airfoil pitching about the quarter-chord point. The particular experimental case of interest studied pitching motion with a reduced frequency, w_r, of 0.202 ($\omega_r = \frac{\omega \cdot chord}{2v_\infty}$, where ω is the angular frequency of the pitching), $M_\infty = 0.796$, a mean angle of attack of 0 degrees, and a maximum pitch angle of 1.01 degrees. The numerical simulation was performed with 25 times steps per period for a total of 10 periods on a structured O-mesh (160 x 32 nodes) with 160 nodes along the airfoil surface. Fig. 6 shows a comparison of the lift coefficient versus angle of attack between SU^2 and experiment during the final period of oscillation. In physical time, the curve is traversed in a counterclockwise fashion. Note that non-linear behavior corresponding to moving shock waves results in a hysteresis effect. The numerical results agree well

with experimentally measured values and also compare favorably with other inviscid results.

In order to verify the accuracy of the gradient information obtained via the time-accurate flow adjoint, 38 Hicks-Henne bump functions were chosen as design variables along the upper and lower surfaces of the NACA 64A010. After solving the adjoint equations using the stored solution data from the numerical experiment performed above, a comparison was made between the gradients of the time-averaged C_d with respect to the design variables calculated using the continuous adjoint and a finite differencing approach with small step sizes for the bump deformations. The gradients compare favorably, although there are slight differences between the adjoint and finite differencing results, as seen in Fig. 6. These small differences are typical for this type of comparison, and it is expected that as the mesh is further refined, the gradients will collapse onto one another.

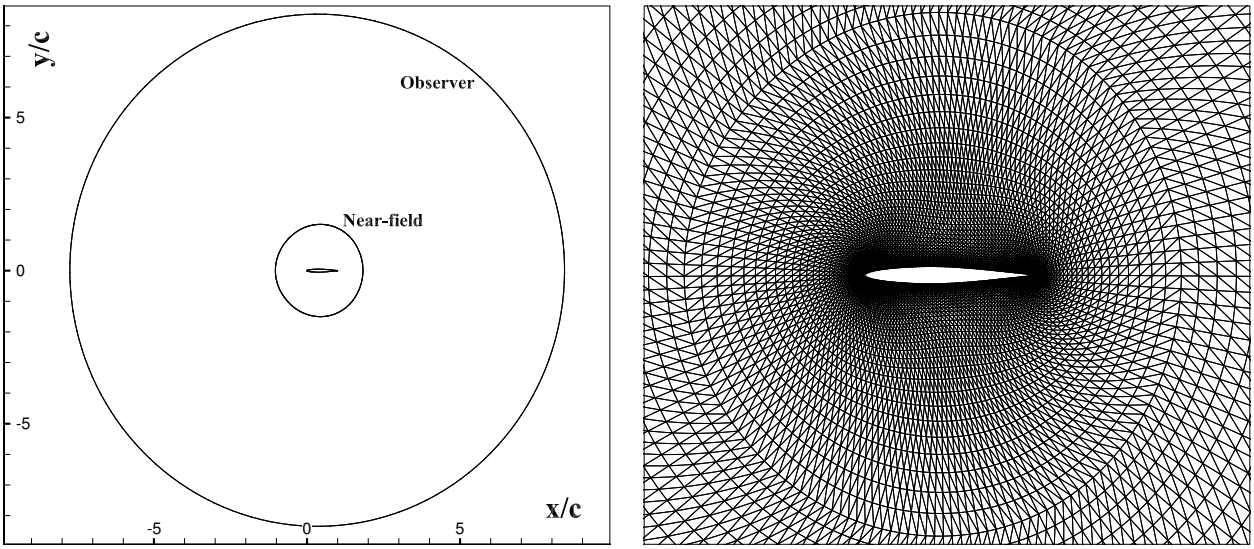

(a) View of the airfoil (center), near-field, and observer surfaces. The x and y coordinates are non-dimensionalized by the airfoil chord length, which is here denoted as c.

(b) Zoom view of the CFD mesh near the airfoil.

Figure 7. Views of the two mesh system for the CFD and CAA problems.

B. Demonstration of Remote Sensitivities for Noise Control

While the previous results made use of CFD alone, for demonstrating the coupled-adjoint methodology, a single shape design cycle was performed for minimizing the observed noise of the NACA 64A010 airfoil pitching in still air. Two overlapping grids were created for the CFD and CAA problems, as shown in Fig. 7. The coupling between the CFD and CAA occurred at the near-field, Γ_{nf}, and the noise was observed in the CAA solver at Γ_{obs}. A true far-field boundary, Γ_∞, was placed many body-lengths away such that no reflections were observed in either solver. The meshes are identical external to Γ_{nf}.

The numerical experiment entailed sending a single pulse into the domain using a nose-down pitching motion, and the noise was computed as the square of the acoustic pressure at Γ_{nf} due to the pulse. Examples of the coupled analysis are shown in Fig. 8 for two different time steps. With each physical time step in the dual-time stepping solvers, the CFD and CAA solutions are tightly coupled at the interface through the FW-H source terms, and this coupling is evident in the close alignment of the density contours across the two domains, as seen in Fig. 8.

Using the stored solution data from the coupled analysis problem, the coupled-adjoint solution was computed. During the coupled-adjoint simulation, disturbances propagate inwards toward the center of the domain starting from Γ_{nf}. These disturbances move through the adjoint CAA domain until they are transferred to the adjoint CFD domain via the new coupling boundary condition and eventually reach the airfoil surface where the surface sensitivity is computed at each time step. In order to calculate the gradient, the time-averaged surface sensitivities to the noise were then projected into a design space composed of the same 38 Hicks-Henne bump functions used above. After a single step in the gradient direction provided

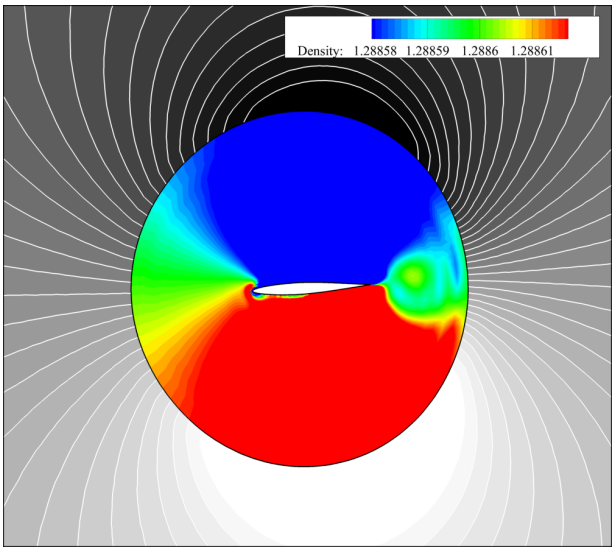

(a) Density contours in the CFD (color) and CAA (grey) solutions at $t = 0.1649$ in a nose-down pitching position.

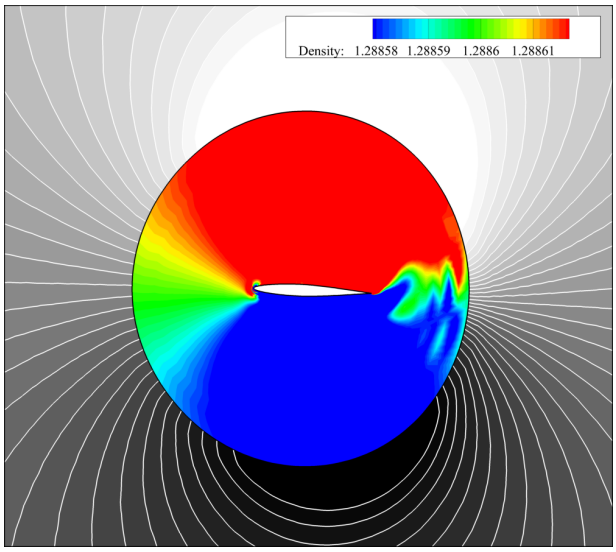

(b) Density contours in the CFD (color) and CAA (grey) solutions at $t = 0.2662$ in a nose-up pitching position.

Figure 8. Example solutions in both the CFD and CAA solvers during the coupled analysis problem.

a new set of design variable values for the bumps, the mesh was deformed, and a new coupled analysis was performed. A comparison of the baseline and deformed airfoil shapes, as well as the resulting noise signatures versus time for the pulse, are presented in Fig. 9. The coupled-adjoint method successfully provided a gradient that reduces the observed total noise by 1.87% after a single design cycle, mostly due to a thinning of the airfoil profile. This agrees with intuition, as a thinner airfoil should displace a smaller volume of fluid and thus produce less thickness noise.

VII. Conclusions

The simple demonstration of the coupled-adjoint for a pitching airfoil is just a starting point for our investigation into the control of noise. This article has presented a methodology for addressing aerodynamics and aeroacoustics via separate numerical methods coupled within a single design framework. Time-accurate continuous adjoint formulations have been developed for both aerodynamics and aeroacoustics, and furthermore, these formulations have been coupled through a new type of boundary condition to offer a designer remote sensitivity information. This results in an efficient, adjoint-based methodology for multiphysics design problems. The method was applied to aeroacoustic shape design where the noise of a pitching airfoil observed at an off-body location was successfully reduced using gradient information obtained using the coupled-adjoint.

Future work will aim to extend several aspects of the present coupled-adjoint methodology. Boundary integral methods will be considered for solving the CAA analysis and adjoint problems. Other aeroacoustic objective functions will also be investigated, such as the inverse design of acoustic signatures or controlling the directionality of noise through tailoring the shape and location of Γ_{obs}, which could have many interesting applications for aerospace systems. Adding more geometric complexity, fidelity, or physics should not change the methodology. For instance, a designer could easily include more physics by choosing the Reynolds-averaged Navier-Stokes (RANS) equations in the CFD domain while leaving the overall coupled design framework unchanged. Furthermore, the method has been developed in a general manner such that it could be applied to other multiphysics problems where adjoint sensitivities are desired for use in optimal shape design, error estimation, or goal-oriented mesh adaptation, for example.

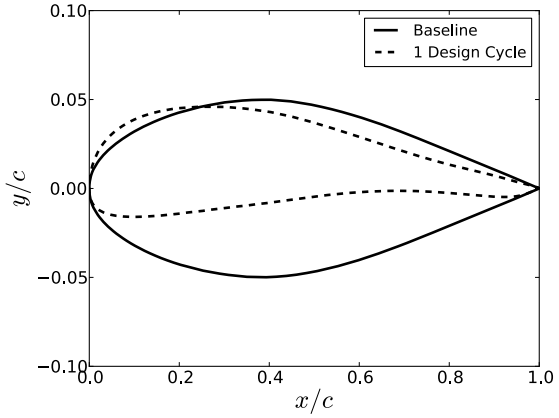

(a) Airfoil profile comparison after one design cycle using the gradient from the coupled-adjoint to deform the Hicks-Henne bumps along the surface. Airfoil chord again denoted by c.

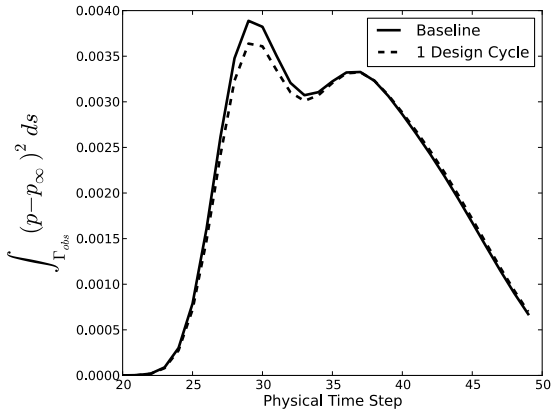

(b) Comparison of the acoustic pressure over time for the baseline airfoil and the new shape after one design cycle. The time-average of the total noise over the interval was reduced by 1.87%.

Figure 9. Numerical results after one design cycle using the coupled-adjoint methodology.

VIII. Acknowledgements

T. Economon would like to acknowledge U.S. government support under and awarded by DoD, Air Force Office of Scientific Research, National Defense Science and Engineering Graduate (NDSEG) Fellowship, 32 CFR 168a.

References

[1]Jameson, A., "Aerodynamic Design Via Control Theory," *AIAA 81-1259*, 1981.

[2]Jameson, A., Alonso, J. J., Reuther, J., Martinelli, L., Vassberg, J. C., "Aerodynamic Shape Optimization Techniques Based On Control Theory," *AIAA-1998-2538*, 29th Fluid Dynamics Conference, Albuquerque, NM, June 15-18, 1998.

[3]Anderson, W. K. and Venkatakrishnan, V., "Aerodynamic Design Optimization on Unstructured Grids with a Continuous Adjoint Formulation," *Journal of Scientific Computing*, Vol. 3, 1988, pp. 233-260.

[4]Nadarajah, S. K., Jameson, A., "Optimum Shape Design for Unsteady Flows with Time-Accurate Continuous and Discrete Adjoint Methods," *AIAA Journal*, Vol. 45, No. 7, pp. 1478-1491, July, 2007.

[5]Nielsen, E. J., Diskin, B., "Discrete Adjoint-Based Design for Unsteady Turbulent Flows On Dynamic Overset Unstructured Grids," *AIAA-2012-0554*, 50th AIAA Aerospace Sciences Meeting including the New Horizons Forum and Aerospace Exposition, Nashville, Tennessee, Jan. 9-12, 2012.

[6]Rumpfkeil, M. P., Zingg, D. W., "Unsteady Optimization Using a Discrete Adjoint Approach Applied to Aeroacoustic Shape Design," *AIAA-2008-18*, 46th AIAA Aerospace Sciences Meeting and Exhibit, Reno, NV, Jan. 7-10, 2008.

[7]Bueno-Orovio, A., Castro, C., Palacios, F., and Zuazua, E., "Continuous Adjoint Approach for the Spalart-Allmaras Model in Aerodynamic Optimization," *AIAA Journal* , Vol. 50, No. 3, pp. 631-646, March 2012.

[8]Economon, T. D., Palacios, F., Alonso, J. J., "Optimal Shape Design for Open Rotor Blades," *AIAA-2012-3018*, 30th AIAA Applied Aerodynamics Conference, New Orleans, Louisiana, June 25-28, 2012.

[9]Ffowcs Williams, J. E., Hawkings, D. L., "Sound Generation By Turbulence and Surfaces in Arbitrary Motion," *Philosophical Transactions of the Royal Society of London*, A 342, pp.264-321, 1969.

[10]Alonso, J. J., Kroo, I. M., Jameson, A., "Advanced Algorithms for Design and Optimization of Quiet Supersonic Platforms," *AIAA-2002-0144*, 40th AIAA Aerospace Sciences Meeting and Exhibit, Reno, NV, Jan. 14-17, 2002.

[11]Jameson, A., Schmidt, W., and Turkel, E., "Numerical Solution of the Euler Equations by Finite Volume Methods Using Runge-Kutta Time-Stepping Schemes," *AIAA 81-1259*, 1981.

[12]Jameson, A., "Time Dependent Calculations Using Multigrid, with Applications to Unsteady Flows Past Airfoils and Wings," *AIAA 91-1596*, 10th AIAA Computational Fluid Dynamics Conference, Honolulu, Hawaii, June 24-26, 1991.

[13]Hicks, R. and Henne, P., "Wing design by numerical optimization," *Journal of Aircraft*, Vol. 15, pp. 407-412, 1978.

[14]Degand, C. and Farhat, C., "A three-dimensional torsional spring analogy method for unstructured dynamic meshes, *Computers & Structures*, Vol. 80, pp. 305-316, 2002.

[15]Davis, S. S., "NACA 64A010 (NASA Ames model) Oscillatory Pitching, Compendium of Unsteady Aerodynamic Measurements, AGARD, Rept. R-702, Neuilly sur-Seine, France, Aug. 1982.